

Visualization of flow patterning in high-speed centrifugal microfluidics

Markus Grumann,^{a)} Thilo Brenner, Christian Beer, Roland Zengerle, and Jens Ducee
*IMTEK-University of Freiburg, Laboratory for MEMS Applications, Georges-Koehler-Allee 106,
 D-79110 Freiburg, Germany*

(Received 11 February 2004; accepted 4 October 2004; published online 6 January 2005)

This work presents a new experimental setup for image capturing of centrifugally driven flows in disk-based microchannels rotating at high frequencies of up to 150 Hz. To still achieve a micron-scale resolution, smearing effects are minimized by a microscope-mounted CCD camera featuring an extremely short minimum exposure time of 100 ns, only. The image capture is controlled by a real-time PC board which sends delayed trigger signals to the CCD camera and to a stroboscopic flash upon receiving the zero-crossing signal of the rotating disk. The common delay of the trigger signals is electronically adjusted according to the spinning frequency. This appreciably improves the stability of the captured image sequences. Another computer is equipped with a fast framegrabber PC board to directly acquire the image data from the CCD camera. A maximum spatial resolution ranging between 4.5 μm at rest and 10 μm at a 150 Hz frequency of rotation is achieved. Even at high frequencies of rotation, image smearing does not significantly impair the contrast. Using this experimental setup, the Coriolis-induced patterning of two liquid flows in 300- μm -wide channels rotating at 100 Hz is visualized at a spatial resolution better than 10 μm .
 © 2005 American Institute of Physics. [DOI: 10.1063/1.1834703]

I. INTRODUCTION

Microfluidic technologies play a key role for enabling many novel applications in the life sciences.^{1–6} End-users in these fields request technology platforms which provide mature solutions for a given group of applications, for instance the drug discovery pipeline or the gene expression workflow. These market needs are addressed by “lab-on-a-chip” systems which integrate basic analytical steps such as sample injection, preparation, amplification and detection to perform complex diagnostic tasks on a credit-card sized, microfluidic substrate.^{7–11}

A special type of these lab-on-a-chip devices are microstructured disks, so called “labs-on-a-disk,” which were published for the first time by the group of Madou in 1998.^{6,12–15} Set into spinning motion, these disks transport liquid by means of the centrifugal force from inlets near the center of the disk through preferentially radial microchannels to the outer perimeter (Fig. 1). Basic operations such as stopping and mixing of flows commonly result from the intricate interplay of the centrifugal force with the geometry and hydrophobic patterning of the microfluidic structures.^{16–18}

Compared to conventional lab-on-a-chip devices, these modular lab-on-a-disk platforms display several intrinsic advantages: First, the actuation and the detector as well as all moving parts are entirely delegated to a robust macroscopic unit which resembles a conventional CD-ROM drive. The microfluidic disk thus constitutes a merely passive module, avoiding the error-prone hybrid or monolithic integration. Second, the mechanical interface between the two system modules is constituted by a simple macroscopic disk holder.

The fluidic macro-to-micro interfacing, i.e., the introduction of liquid at the inlet ports, is supported by the centrifugal field. Finally, as for other lab-on-a-chip technologies, the detection, e.g., by optical readout, can be performed by conventional equipment with the disk at rest.

In summary, the lab-on-a-disk platform possesses a great potential for a comprehensive process integration of liquid handling and detection in diagnostic assays^{19–22} and also synthetic applications.²³ Combined with their robustness and simplicity, they are deemed a promising candidate for a successful commercialization.

In this work, we present a new, high-performance experimental setup which is able to accurately visualize microscale flow patterns on disks at a maximum resolution be-

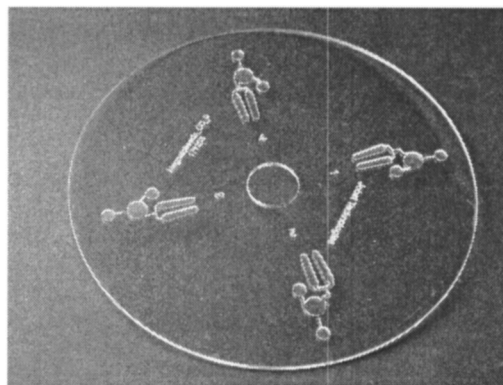


FIG. 1. Microstructured “lab-on-a-disk” featuring four parallel mixing devices. All disks are made of PMMA with an outer diameter of 120 mm, an inner (hole) diameter of 15 mm, and a thickness of 1.6 mm. The prototyping by precision machining imposes a minimum lateral structure width of 200 μm . Sealing is achieved either by a self-adhesive PDMS cover or by lamination of scotch tape.

^{a)} Author to whom correspondence should be addressed; electronic mail: grumann@imtek.de, www.imtek.de/anwendungen/

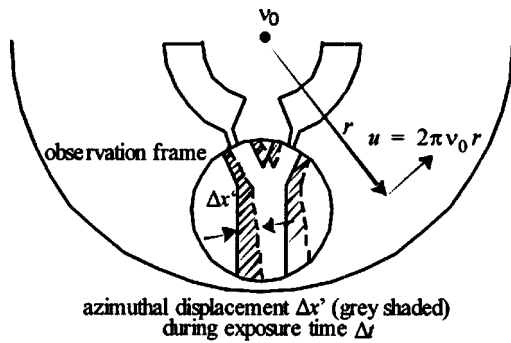


FIG. 2. Azimuthal displacement $\Delta x'$ ("smearing") observed in a magnified frame on a disk featuring microfluidic structures and rotating at ν_0 during a CCD camera exposure time Δt . u denotes the speed of a point spaced by the radius r from the center of rotation in the lab frame.

tween $4.5 \mu\text{m}$ at rest and $10 \mu\text{m}$ during rotation at 150 Hz. The setup is composed of a CCD camera with an ultrashort, 100 ns (minimum) exposure time, a microscope and a stroboscopic flash as well as two PCs for real-time frequency control, triggering and data storage. At rest, the resolution of $4.5 \mu\text{m}$ is primarily limited by the optical microscope and the CCD camera. During spinning motion, images are smeared out by an azimuthal displacement derived to be $4.7 \mu\text{m}$ for 150 Hz.

With this setup, we demonstrate the visualization of flow patterning in spinning microchannels by the previously discovered secondary transversal flow patterns arising in radial channel networks under the impact of the apparent Coriolis force.^{24–26} These transversal currents arise as the Coriolis pseudoforce, which is experienced by the liquid in the non-inertial disk-frame, dominates all other forces, including the centrifugal force. In a radial channel with a radius of $200 \mu\text{m}$ and water as liquid, the apparent Coriolis force prevails the centrifugal force for frequencies above $\nu_0=14$ Hz. To still observe resulting microstructured flow patterns towards high speeds of rotation, the optical smearing during the finite exposure time of the CCD camera must remain significantly smaller than the actual width of the pattern, in this case some 10 microns, to be observed.

II. REQUIREMENTS ON MEASUREMENT SETUP

The chief aim of the setup is to obtain a stable and magnified image of the flow patterns within the microstructures on the rapidly rotating disk. The azimuthal displacement of each captured frame $\Delta x'$ in the corresponding image plane ("smearing"), which is linked to the finite exposure time of the CCD camera Δt , has to be minimized for high-resolution pictures. This way, a point located at a distance r from the center of a channel moves at a lab-frame velocity

$$\Delta x' / \Delta t = 2\pi\nu_0 \cdot r \quad (1)$$

while rotating at frequency ν_0 (Fig. 2). For instance, an object positioned at $r=5$ cm and rotating at $\nu_0=100$ Hz travels at a speed of 31.4 m s^{-1} in the lab frame! Under these experimentally most challenging conditions, a maximum exposure time $\Delta t = \Delta x' / 2\pi\nu_0 r < 320$ ns is necessary to reach a theoretical spatial resolution $\Delta x' = 10 \mu\text{m}$.

III. EXPERIMENTAL SETUP

The measurement setup consists of a modified compact disk player ("Bio-Disk player") and an image capturing unit (Fig. 3). The PC-controlled *Bio-Disk* player spins the disk at a defined frequency of rotation up to $\nu_0=150$ Hz. The image capturing unit is composed of a stroboscopic flash [Drelloscope 255-01, Drello GmbH (Ref. 27)] and a CCD camera [Sensicam fast shutter, PCO Computer Optics GmbH (Ref. 28)] which is mounted on a microscope [Leica MZ12.5, Leica Microsystems GmbH (Ref. 29)] to obtain a tenfold magnification of the captured image. The high speed CCD camera allows very short exposure times down to 100 ns. As the changes in the microfluidic processes under investigation proceed on time scales in the range of seconds, the image capture rate ν is of minor importance.

During the nonexposure period, the CCD chip can only be blocked electronically which turns out to be insufficient to rule out a weak acquisition of light. Thus, the light accumulated over the nonexposure time produces a parasitic background in the captured image. The background can become dominant for very short exposure times Δt compared to the full period T_0 . To reduce this effect, i.e., to enhance the con-

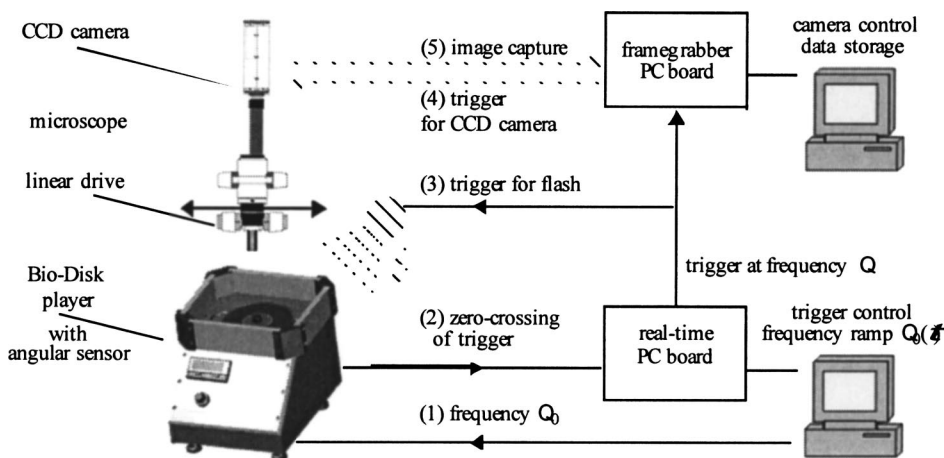


FIG. 3. The experimental setup is composed of the Bio-Disk player, a microscope, a CCD camera, a stroboscopic flash and two PC boards. CCD camera and trigger control are implemented by a framegrabber and a real-time PC board, respectively. The spinning frequency ramp $\nu_0(t)$ is set by a custom-made graphical-user-interface (GUI) and then sent to the player (1). Next, the zero-crossing trigger signal of the angular sensor in the player is AD-converted and processed by a real-time PC board (2). This PC board subsequently triggers the stroboscopic flash (3) and the CCD camera (4) at the frequency ν . The acquired frames are transiently recorded by the framegrabber PC board and then forwarded to the PC RAM (5).

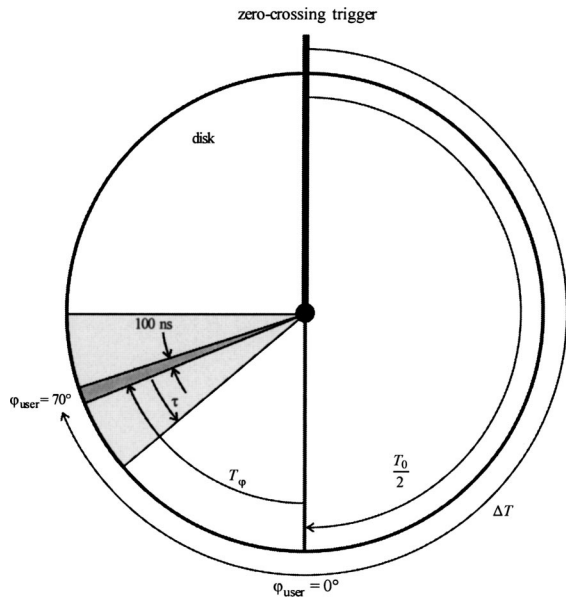


FIG. 4. Active trigger control. A nominal angular shift φ_{user} of 70° is transferred into a delay time $\Delta T = T_0/2 + T_\varphi$ which is composed of a constant half period $T_0/2$ and the additional delay T_φ . Additionally, an offset τ of $12.8 \mu\text{s}$ has to be subtracted from T_φ because the stroboscopic flash needs to be triggered $12.8 \mu\text{s}$ in advance to obtain its maximum intensity during exposure of the camera. To achieve a best-case image resolution, the exposure time of the CCD camera is set to its minimum value of 100 ns .

trast, a stroboscopic flash is used which clearly exceeds the intensity of the background light during the exposure time.

Two PCs control the setup. The first PC is equipped with a framegrabber PC board [PCI-board 525KP1573, PCO Computer Optics GmbH (Ref. 30)] to manage the time critical acquisition of image data from the 1280×1024 pixel CCD chip at a maximum operating frequency of $\nu_{\text{max}} = 8 \text{ Hz}$. The second PC features a real-time PC board (ADwin-light-16, Jaeger Computergesteuerte Meßtechnik GmbH, Lorsch, Germany³¹) for controlling the setup components. The zero-crossing signals from the player are forwarded with different, preselected delays (Fig. 3) to the framegrabber PC board (CCD camera and data storage), and to the stroboscopic flash. The user directly interacts with the

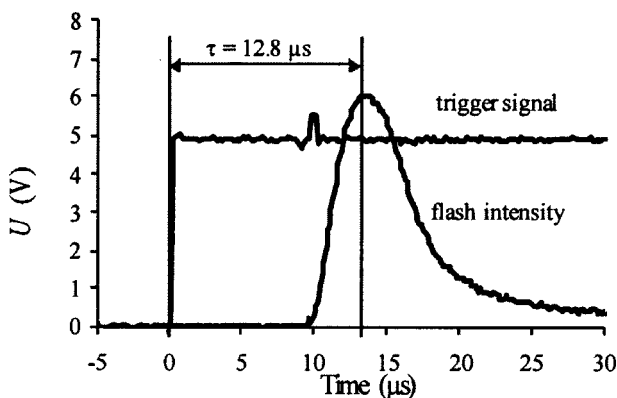


FIG. 5. Intensity distribution of the flash after triggering. The experimental data is obtained by acquiring the signal U of a fast-response diode with an oscilloscope and subsequent signal processing via PC. This way, τ is determined as the distance between the rising edge of the trigger signal and the maximum intensity of the flash.

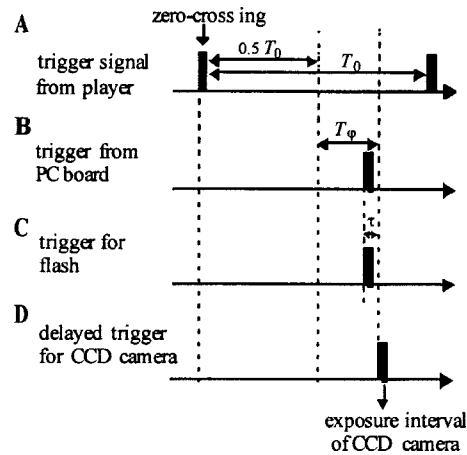


FIG. 6. Concept of the time-critical signal-processing: The trigger signal which is generated by the angular sensor in the player (A) at a period T_0 is forwarded to the real-time PC board (B). This board computes an additional delay T_φ according to the user-selected azimuthal position of the CCD camera and subtracts the constant flash delay τ to synchronize the stroboscopic flash and the CCD camera. Thus, it is guaranteed that the CCD camera shoots at the maximum intensity of the flash (D).

experiments by a comfortable graphical user interface (Testpoint 4.1, Keithley Instruments GmbH, Germany³²). The whole capturing unit can be positioned by software at user selected radial and azimuthal positions by a linear mechanical drive with a tolerance of $10 \mu\text{m}$. This allows a capturing of images at arbitrary positions on the disk. Furthermore, the user can set acceleration ramps, delays and time intervals of constant rotational frequency. All these settings can be stored on the PC in a user-defined protocol.

The image capturing unit is triggered by the zero-crossing signal of the rotating disk. An optical angular sensor attached to the player detects the periodical zero-crossing of the rotating disk and forwards the trigger-signal to a real-time PC board. The rotating frequency

$$\nu_0 = \frac{1}{T_0} \tag{2}$$

is derived from the time interval T_0 between two signals. An integer scaler adjusts the rate of image capture

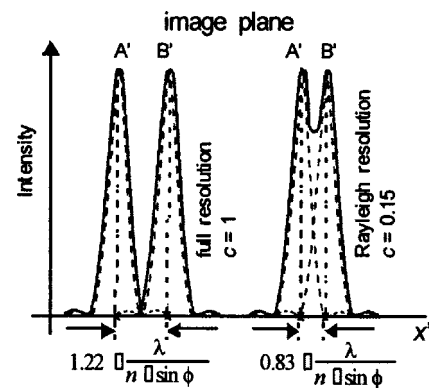


FIG. 7. Spatial resolution of two incoherently luminescing point-like objects A and B with completely resolved corresponding images A' and B' ($c=1$, left) and partly resolved images following the Rayleigh criterion ($c=0.15$, right). The Rayleigh criterion is satisfied when the center of the diffraction pattern A' (Airy disk) of object A coincides with the first minimum of the diffraction pattern B' of object B.

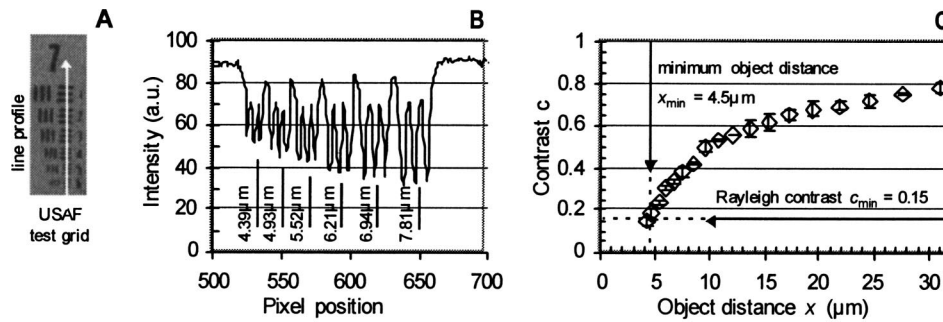


FIG. 8. Evaluation of the maximum spatial resolution at rest: To experimentally determine the minimum resolvable object distance x_{\min} , a USAF high-precision test-target which features a manifold of line pairs at different (known) spacings is used (A). Here, each test object comprises three opaque lines at a defined width spaced by two transparent lines of the same width. These objects are classified by the nominal number of line pairs per mm which corresponds to the object distance x in a reciprocal way. All images of the test-target are captured at tenfold optical zoom and tenfold digital zoom. Line profiles of all beam-structures are drawn and the maximum and minimum values of the intensity distribution are identified (B). Using Eq. (6) and assuming the Rayleigh-criterion $c=0.15$ to determine the limit of resolution, a maximum spatial resolution x_{\min} of $4.5 \mu\text{m}$ is obtained (C).

$$\nu = (\nu_0 \text{ MOD } 8) + 1 \text{ Hz} \quad (3)$$

to comply with the maximum operating frequency $\nu_{\max} = 8 \text{ Hz}$ of the CCD camera.

Active real-time trigger control is required to achieve spatial stability of the picture (“freeze image”) at varying frequencies and to set the frame of observation to the preselected angular positions on the disk. The trigger is further adapted to individual electronic delays of the setup components. According to the frequency of rotation ν_0 and the user-defined angular position φ on the disk, the trigger signal is delayed by

$$\Delta T(\nu, \varphi) = \frac{T_0}{2} + T_\varphi - \tau = \frac{1}{2\nu_0} + T_0 \frac{\varphi}{360^\circ} - \tau \quad (4)$$

on the PC board. $\Delta T(\nu, \varphi)$ consists of a constant delay of half a period $T_0/2$ and an additional time T_φ according to the preselected angular position φ to be observed (Fig. 4).

Furthermore, an offset τ is subtracted from that delay in order to compensate the response time of the flash. This time offset was obtained by measuring the output signal of a photodiode facing the optical output interface of the flash. A time offset $\tau = 12.8 \mu\text{s}$ was measured by an oscilloscope between the rising edge of the trigger signal (upper line) and the

maximum light intensity (lower line) (Fig. 5). This way, the stroboscopic flash is triggered at a time interval τ prior to the exposure of the CCD camera.

At $\varphi_{\text{user}} = 0$, the capture is taken at a half period $T_0/2$ of rotation of the disk after the zero-crossing. This constant offset is necessary to allow a signal processing time prior to triggering of the flash. Otherwise the flash may possibly be triggered before the zero-crossing signal of the player. $T_0/2$ always amounts to more than $12.8 \mu\text{s}$, even at frequencies of 100 Hz . The PC board then forwards the signal to the flash light and, with an additional trigger delay $\tau = 12.8 \mu\text{s}$, to the controller of the CCD camera. The captured pictures are stored to the PC RAM and saved in standard file format. Figure 6 shows the time diagram of all trigger delays at the PC board and the CCD camera.

IV. EVALUATION OF THE SPATIAL RESOLUTION

To evaluate the limits of spatial resolution at rest and during rotation, two appropriate test structures are optically analyzed. Additionally, theoretical calculations are carried out to verify the identified limitations.

Following the Rayleigh-criterion, two equally bright points A and B in the object plane are spatially resolvable

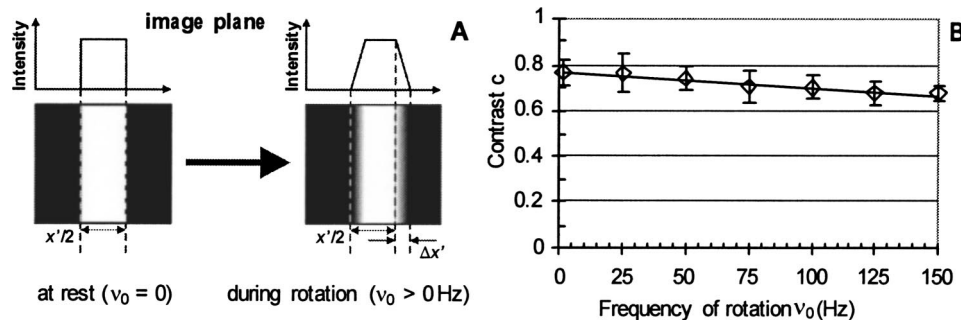


FIG. 9. Evaluation of the maximum spatial resolution during rotation: A test-structure with periodically arranged opaque beams and transparent spacing at a linewidth x of $30 \mu\text{m}$ is recorded at varying frequencies of rotation ν_0 . The distance r of the test-structure to the center of rotation amounts to 5 cm , the exposure time of the CCD camera Δt was kept at 100 ns . (A) In the image plane, the nearly rectangular intensity profile observed for the disk at rest distorts to a trapezoid with lateral ramps at a width $\Delta x'$. The overall broadening of the recorded feature size x' roughly corresponds to the azimuthal path the object travels during rotation [Eq. (1)]. Experimentally, the contrast of 0.77 at rest diminishes to 0.67 at 150 Hz which is still sufficient to resolve the flow patterns in the centrifugal flows.

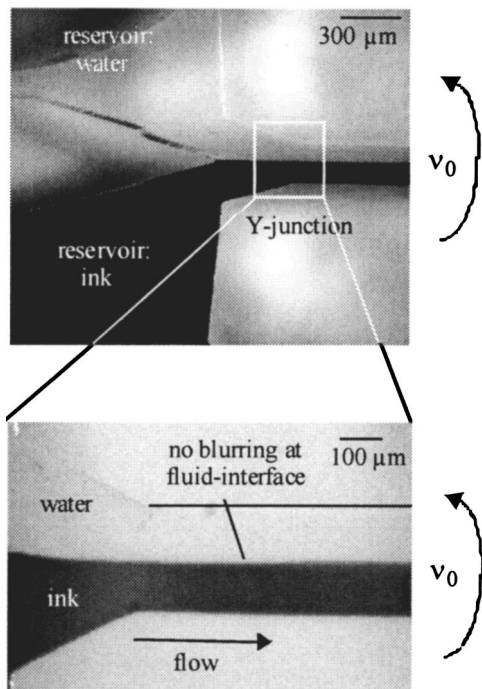


FIG. 10. Laminar flow of water and ink in a microfluidic channel rotating at $v_0=100$ Hz. The microfluidic structure is manufactured by micromachining and sealed with scotch tape (Ref. 24). The geometrical dimensions of the mixing channel (see inset) are $300\ \mu\text{m}$ in width and $65\ \mu\text{m}$ in depth. By the Coriolis force, the centrifugally driven liquid streams are laminated perpendicular to the direction of flow (Ref. 23).

when the first minimum of the corresponding diffraction pattern A' in the image plane coincides with the maximum of the diffraction pattern B'.

For noncoherent illumination, this leads to a minimum resolvable object spacing

$$x_{\min} = 0.83 \cdot \frac{\lambda}{n \cdot \sin \phi} \quad (5)$$

with the wavelength of the exposed light λ , the numerical aperture of the objective lens $\sin \phi$ and the refractive index n of the medium between the sample and the objective lens (Fig. 7). With the intensity I_{\max} of the image of the bright points A and B and the intensity I_{\min} of the corresponding dark intermediate area, the contrast

$$c = \frac{(I_{\max} - I_{\min})}{(I_{\max} + I_{\min})} \quad (6)$$

possesses a minimum value $c_{\min}=0.15$ at the maximum theoretical resolution defined by the Rayleigh criterion.

With a numerical aperture of $\sin \phi=0.125$ of the objective lens, a wavelength of $\lambda=480$ nm, and the refractive index n of air leads to a minimum resolvable feature size x_{\min} of $3.2\ \mu\text{m}$. However, in practice, this limitation is only reached for a precisely adjusted optical beampath. Additionally, the spectrum of the thermal light source²⁷ used for the illumination of the objects covers the complete visible range, i.e., also wavelengths λ larger than 480 nm, to deteriorate the resolution.

To determine the experimental resolution x_{\min} , a high-precision test target³³ featuring a series of line pairs at known

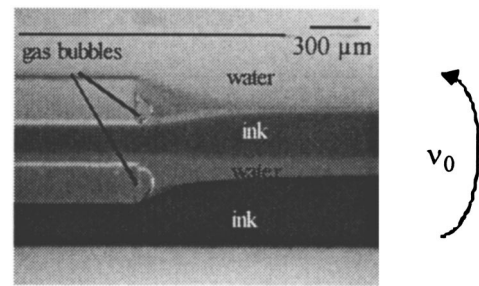


FIG. 11. Sequence of concurrent flows at $v_0=100$ Hz. Exploiting the Coriolis force acting perpendicular to the centrifugal force, two fluids can be laminated, thus their mixing can be enhanced (Ref. 26).

spacings is placed in the object plane of the microscope [Fig. 8(A)]. Subsequently, an intensity profile is generated from the images captured by the attached CCD camera [Fig. 8(B)] to eventually calculate the contrast c as a function of the line spacing using Eq. (6) [Fig. 8(C)]. According to the Rayleigh criterion, the minimum resolvable feature size x_{\min} corresponds to $c_{\min}=0.15$ as indicated by the dashed horizontal line in Fig. 8(C). Hence, a spatial resolution x_{\min} of roughly $4.5\ \mu\text{m}$ is determined [vertical arrow in Fig. 8(C)] which is in good agreement with the result of the previously derived theoretical value of $3.2\ \mu\text{m}$.

In order to determine the decrease of spatial resolution during rotation, it is not possible to use the previous standard technique as the mechanical stress would bear a high risk of destroying the expensive glass target. Instead, a high-resolution (5080 dpi), periodical beam-structure is plotted³⁴ and fixed on a disk. Here, the selected line pair width x of $30\ \mu\text{m}$ displays a lower limit of typical microfluidic structures. The radius of the orbit which is generated by the rotating test structure amounts to 5 cm. At a frequency ν_0 of 150 Hz and an exposure time of 100 ns for example, an azimuthal displacement $\Delta x'$ of $4.7\ \mu\text{m}$ occurs in the corresponding image plane [Eq. (1)], i.e., the nearly rectangular intensity-profile of the beam-structure measured at rest distorts to a trapezoidal shape to broaden the width at half-maximum during rotation [Fig. 9(A)]. Thus, a decay of the contrast c with increasing frequency ν_0 is expected and indeed verified by the experiments [Fig. 9(B)]: at rest, a contrast c of 0.77 is measured, decreasing $c=0.67$ at an extremely high frequency of 150 Hz. However, this decrease does not significantly worsen the resolution of the $30\ \mu\text{m}$ features that are typical for the following observation of Coriolis-induced flow patterns in microchannels.

In summary, the experimentally determined spatial resolution of x_{\min} at $4.5\ \mu\text{m}$ denotes the maximum theoretical resolution of the optical system. The rotation does not impair this performance significantly, since the ultrashort exposure time keeps smearing effects ($\Delta x'$) in the range of the limit of resolution x_{\min} .

V. VISUALIZATION OF FLOW PATTERNS

To prove the performance of the experimental setup, the concurrent, centrifugally driven flow of two adjacent liquids at a Y-junction of a channel rotating at 100 Hz is monitored at high accuracy (Fig. 10). Even at such a high speed, no

blurring of the fluidic interface between water and black ink can be seen at the entrance of the common channel. Note that mixing takes place under the impact of the Coriolis force.^{24,26} Note also that the observation of the lamination patterns in Fig. 11 is enabled by the high resolution delivered by the experimental setup. Since the CCD camera and the attached microscope can be moved by a linear drive, the temporal evolution of the flow patterning along the entire channel can be recorded.

ACKNOWLEDGMENTS

The authors are grateful to the support by the Ministry of Science, Research and the Arts of the German federal state of Baden-Wuerttemberg and the good cooperation with HSG-IMIT and Jobst Technologies.

- ¹D. Reyes, D. Iossifidis, P. Auroux, and A. Manz, *Anal. Chem.* **74**, 2623 (2002).
- ²P. Auroux, D. Reyes, D. Iossifidis, and A. Manz, *Anal. Chem.* **74**, 2637 (2002).
- ³*Micro Total Analysis Systems*, edited by A. van den Berg and E. Oosterbroek (Elsevier Science, Amsterdam, 2003).
- ⁴myFluidix.com—Free Online Resources in Microfluidics—myfluidix.com June 2003.
- ⁵*FlowMap—Microfluidics Roadmap for the Life Sciences*, edited by J. Duce, R. Zengerle www.microfluidics-roadmap.com Books on Demand GmbH (Norderstedt, Germany, 2004).
- ⁶M. Madou and G. Kellogg, *Proc. SPIE* **3259**, 80 (1998).
- ⁷L. Bousse, S. Mouradian, A. Minalla, H. Yee, K. Williams, and R. Dubrow, *Anal. Chem.* **73**, 1207 (2001).
- ⁸D. Figeys and D. Pinto, *Electrophoresis* **22**, 208 (2001).
- ⁹Shimadzu Biotech—www.shimadzu-biotech.net December 2003.
- ¹⁰J. Khandurina, T. McKnight, S. Jacobson, L. Waters, R. Foote, and J. Ramsey, *Anal. Chem.* **72**, 2995 (2000).
- ¹¹T. Thorsen, S. Maerkl, and S. Quake, *Science* **298**, 580 (2002).
- ¹²M. Madou, Y. Lu, S. Lai, J. Lee, and S. Daunert, *Proceedings of the MicroTAS 2000 Conference*, edited by A. van den Berg and P. Bergveld (Kluwer Academic, Dordrecht, 2000), pp. 565–570.
- ¹³M. Madou, Y. Lu, S. Lai, C. Koh, Y.-J. Juang, L. Lee, and B. Wenner, *Sens. Actuators, A* **91**, 301 (2001).
- ¹⁴M. Madou, L. Lee, S. Daunert, S. Lai, and C. Shih, *Biomed. Microdevices* **3**, 245 (2001).
- ¹⁵L. Lee, M. Madou, K. Koelling, S. Daunert, S. Lai, C. Koh, Y.-J. Juang, Y. Lu, and L. Yu, *Biomed. Microdevices* **3**, 339 (2001).
- ¹⁶G. Ekstrand, C. Holmquist, A. E. Örléfor, B. Hellmann, A. Larsson, and P. Andersson, in *Proceedings of the MicroTAS 2000 Conference*, edited by A. van den Berg and P. Bergveld (Kluwer Academic, Dordrecht, 2000), pp. 311–314.
- ¹⁷J. Duce, T. Brenner, M. Grumann, W. Bessler, M. Stelzle, S. Messner, T. Nann, J. Ruehe, I. Moser, and R. Zengerle, *Bio-Disk—A centrifugal platform for integrated point-of-care diagnostics on whole blood—www.bio-disk.com*
- ¹⁸G. Thorsén, G. Ekstrand, U. Sedlitz, S. Wallenborg, and P. Andersson, *Proceedings of the MicroTAS 2003 Conference*, MESA Monographs, pp. 457–460, 2003.
- ¹⁹I. Badr, R. Johnson, M. Madou, and L. Bachas, *Anal. Chem.* **74**, 5569 (2002).
- ²⁰S. Lai, S. Wang, J. Luo, L. Lee, S. Yang, and M. Madou, *Anal. Chem.* **76**, 1832 (2004).
- ²¹LabCD™, Tecan Group Ltd., Switzerland, www.tecan.com
- ²²Gyrolab Bioaffy CD, Gyros AB, Sweden, www.gyros.com
- ²³J. Duce, P. Schlosser, T. Glatzel, and R. Zengerle, *Centrifugal platform for high-throughput reactive micromixing*, accepted at *MicroTAS 2004*, Malmö, Sweden, September 26–30, 2004.
- ²⁴T. Brenner, T. Glatzel, R. Zengerle, and J. Duce, in *Proceedings of the MicroTAS 2003 Conference*, MESA Monographs, pp. 603–606, 2003.
- ²⁵T. Brenner, T. Glatzel, R. Zengerle, and J. Duce, *Lab on a Chip*, 2004, DOI:10.1039/B406699E, 2004.
- ²⁶J. Duce, T. Brenner, T. Glatzel, and R. Zengerle, in *Proceedings of the MicroTAS 2003 Conference*, MESA Monographs, pp. 903–906, 2003.
- ²⁷Drelloscope 255-01, Drello GmbH & Co KG, D-41179 Moenchengladbach, Germany, www.drello.de
- ²⁸Sensicam fast shutter 370KF, PCO Computer Optics GmbH, D-93309 Kehlheim, Germany, www.pco.de
- ²⁹Leica MZ12/5, Leica Microsystems GmbH, Germany, www.leica-microsystems.com
- ³⁰PCI-board 525KP1573, PCO Computer Optics GmbH, D-93309 Kehlheim, Germany, www.pco.de
- ³¹ADwin-light-16, Jaeger Computergesteuerte Meßtechnik GmbH, D-64653 Lorsch, Germany.
- ³²Testpoint 4.1, Keithley Instruments GmbH, Germany, www.keithley.com.
- ³³Melles Griot, resolution test target USAF 1951, product number 04 TRP 003, www.mellesgriot.com 2004.
- ³⁴www.pageworks.com USA, 2004.